Preprint typeset in JINST style - HYPER VERSION

CALICE-CAN-2019-002
October 2th, 2019

# Time Analysis of the Partially Equipped CALICE Analog Hadronic Calorimeter Technological Prototype with Tungsten Absorber

**The CALICE Collaboration***

**This note contains preliminary CALICE results, and is for the use of members of the CALICE Collaboration and others to whom permission has been given.**

ABSTRACT: This note presents the analysis of timing measurements obtained with a partially instrumented technological prototype of the CALICE analog hadronic calorimeter (AHCAL) in a tungsten absorber stack. The data was taken during a test beam campaign in August 2015 at the SPS at CERN. A calibration procedure for time measurements is presented and the complex time structure of hadronic showers is analyzed and compared to several Geant4 physics lists. For pions, late energy depositions are observed as expected due to the capture of low energetic neutrons. Physics lists using the binary cascade to model low energetic hadronic processes underestimate these late energy depositions, while physics lists using the Bertini model or the high precision package overestimate them by about a factor two. The late component of hadronic showers is found to be about eight times larger than for a similar analysis with a steel absorber.

*Corresponding authors: Christian Graf (cgraf@mpp.mpg.de), Frank Simon (fsimon@mpp.mpg.de)

## Contents



## 1. Introduction

The aim of this analysis is to establish a time calibration procedure for the CALICE AHCAL technological prototype, and to study the complex time structure of hadronic showers with this device in a tungsten absorber. The time calibration is similar to [1], but differs in important parts. As the CALICE AHCAL physics prototype was not capable of timing measurements, the T3B experiment [2] did first time measurements parasitic to the physics prototype with a limited number of channels of comparable granularity. For the technological prototype, the ability of time measurements is available for the first time in the whole calorimeter of an CALICE AHCAL prototype. The two test beam campaigns in July and August 2015 at the SPS at CERN were the first opportunity to test these abilities in an environment with high energetic particles. While for the July 2015 test beam campaign a steel absorber stack was used, the August 2015 campaign, relevant for this analysis , used a tungsten absorber stack.

## 2. Experimental Setup

The experimental setup consists of 15 active layers in a tungsten absorber stack, which has 40 equally spaced absorber layers of 10 mm tungsten and 0.5 mm steel support [3, 4]. The first three active layers are single Ecal Base Units (EBUs) with scintillator strips of $4.5 \times 0.5 \times 0.2\,\mathrm{cm}^3$ size instrumented by Hamamatsu MPPCs. The first EBU layer is placed in front of the first tungsten absorber. For the present analysis, the EBU data is not considered. Eight layers of single Hcal Base Unit (HBU) layers with $3 \times 3 \times 0.3\,\mathrm{cm}^3$ scintillator tiles are placed behind the EBUs. Furthermore, four big layers consisting of four HBUs each, are placed with an increased number of empty absorber slots after the single HBU layers. For the HBUs, depending on the layer, scintillator tiles with and without wavelength shifting fibers, as well as different SiPMs are used. A detailed list of the configuration of active layers can be found in appendix A.
Two small and one big trigger scintillators were placed in front of the AHCAL and one big trigger scintillator was placed behind the AHCAL. Additionally, a Cherenkov detector was present in the beam line for particle identification. The coincidence signal of the small trigger scintillators is used as a validation signal and as a time reference. For this purpose six of the channels in the outer part of the big HBUs are used to read out the coincidence signal of the PMTs instrumenting the trigger scintillators, instead of the SiPMs. These channels are called $T_0$-channels. Initially there were six $T_0$-channels foreseen. For the test beam campaign that is discussed in this note, only two of them were working.
Data of 120 GeV muons, 20 GeV electrons and 10, 30, 50, 70 and 90 GeV pions with positive beam polarity are analyzed. The energy reconstruction follows the standard reconstruction procedure and uses the calibration constants that are used in [1].

## 3. Event and Hit Selection

This section briefly describes the event selection for the present analysis. For the validation of events, the $T_0$-channels representing the coincidence of two of the trigger scintillators in front of the AHCAL are used. An amplitude cut on the $T_0$-signals is applied in order to reduce noise in these channels. An event is declared valid if it also has hits in both remaining $T_0$-channels that are within 5 ns (after calibration, see section 4.1). Events that involve two particles from the beam are rejected by identifying hit clusters in the time dimension based on the AHCAL time information. On all hits, a 0.5 MIP cut is applied. As layer 11 was found to be noisy, it is excluded throughout the whole analysis. The chips in layer 12 showed bad TDC spectra and are thus excluded as well for the time analysis.
For Muons, a track is required and a maximum of 20 hits are allowed to ensure non-showering particles. Electrons and hadrons can be distinguished by exploiting the different number of hits in the showers and the position of the shower, as hadrons are expected to shower later than electrons. For this the center of gravity in $z$-direction is used as a discriminative variable. Additionally, a hit in the Cherenkov detector is required for electrons. For hadron beams, the signal of the Cherenkov detector is used to discriminate between pions and protons.

## 4. Time Calibration

Time measurements with the CALICE AHCAL technological prototype are produced in the readout ASIC[1] by a voltage that is ramping up over time with a periodicity of 4 µs. Upon a hit, the current height of the ramp is stored in one of 16 memory-cells and at the end of a read-out cycle digitized by a 12-bit ADC to TDC-values. As the TDC may not be linear at the beginning and at the end of the ramp, only events are selected with the reference time between 500 ns to 3000 ns in order to avoid these edge effects.
The time calibration of the detector consists of several steps. In a first step the reference time, given by the external trigger, needs to be calibrated. Afterwards, the hit times are converted from TDC-values to nanoseconds and further corrections are applied. Each of these steps are described in this section in detail.

As high energetic muons are expected to give quasi-instantaneous energy depositions in the scintillator, muons that go through the detector without the production of any shower are selected for calibration.

### 4.1 Calibration of Reference Time

The aforementioned $T_0$-channels are used as a time reference. The calibration of the time reference is done similar to [1] and will only be described briefly in the following:

The pedestal and the slope of the voltage ramps can be extracted by the TDC-spectra (see e.g., Figure 1(a)). The pedestal is given as the start of the spectrum and the slope can be calculated using the width of the spectrum and the time the ramp needs to reach its maximum (3920 ns, for a ramp up time of 4 µs assuming 2 % dead-time):

$$\text{slope [ns / TDC]} = \frac{3920\,\text{ns}}{\text{Max [TDC]} - \text{Pedestal [TDC]}}. \tag{4.1}$$

The pedestal is determined for each memory-cell of the $T_0$-channels and separately for even and odd bunch crossing IDs. The slope should be stable across the memory-cells and channels of one ASIC. Thus, for the slope, the average of all calculated slopes for all memory-cells is taken as the slope value for this $T_0$-channel (again separately for even and odd bunch crossing IDs). The time of the $T_0$-channels can now be calculated using the slope and the pedestal of the TDC-ramp:

$$t_0[\text{ns}] = (\text{TDC} - \text{Pedestal}) \cdot \text{slope}. \tag{4.2}$$

The time reference is calculated as the mean between both $T_0$-channels:

$$t_{\text{reference}} = \frac{t_{0,1} + t_{0,2}}{2}. \tag{4.3}$$

Figure 1(b) shows the distribution of the differences between both $T_0$-channels. For an event to be valid in the following, the event time reported by the two $T_0$-channels has to be within 5 ns. Additionally, an amplitude cut is applied on the $T_0$-channels to reduce noise.

[1] SPIROC2b [5]

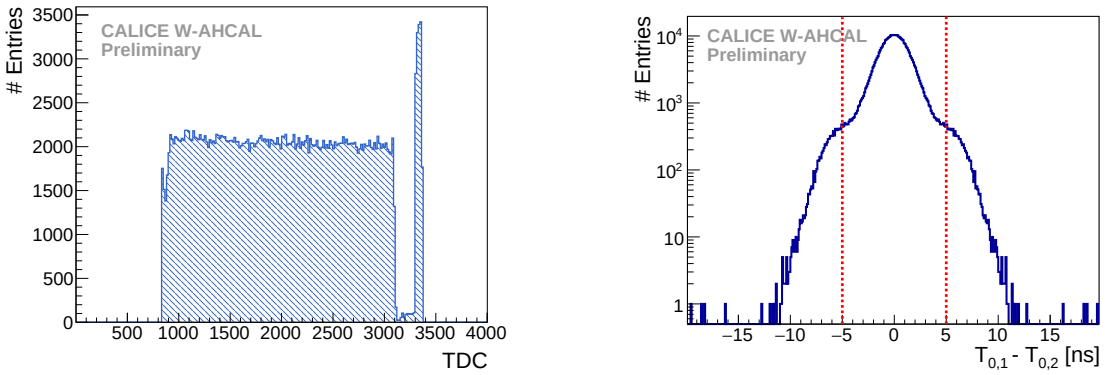


(a) (b)

Figure 1: (a) TDC-spectrum of a representative channel. The gap and the peak in the spectrum between 3000 ns to 3500 ns are due to a malfunction of the electronics. At the end of the TDC cycle, the validation is not working properly and all events are accepted leading to the peak, with a short period of no accepted events before, leading to the gap.(b) Distribution of differences between both $T_0$-channels. The red line marks the cut on the time difference.

### 4.2 Calibration of Hit Time

After the $T_0$-channels are calibrated, each event is assigned a reference time in nanoseconds. The other channels could in principle be calibrated in the same scheme (as it is done for example in [1]). However, as we have already a calibrated time reference for each hit, the correlation between the hit's TDC-value and the reference time can be used for each channel (and memory-cell) (see e.g., fig. 2(a)). This has the advantage that less hits are necessary for the calibration and the procedure is less susceptible to features in the TDC-spectrum. In order to calibrate the channels, a linear fit between the hits TDC-values and its reference times is applied. To reach the necessary precision, this is done in four steps:

1. A robust fit taking 80 % of the hits into account is performed. To avoid edge effects, only the range from 500 to 3000 TDCs is used.

2. Every hit that differs from the prediction of the fit by more than 10 ns is ignored in subsequent fitting steps.

3. As the slope of the TDC-ramp is a feature of the ASIC and should be stable among channels, the average of all such determined slopes of the first memory-cells of all the channels in an ASIC is used as a fixed value for another linear fit.

4. The $y$-interception of this second fit is used as the offset value for this memory-cell.

Again, even and odd bunch crossing IDs are treated separately. This procedure requires at least 30 hits in the corresponding memory-cell and at most 1000 hits are considered. The hit times are then calculated with respect to the $T_0$-reference time as:

$$t\,[\mathrm{ns}] = \mathrm{TDC} \cdot \mathrm{Slope}\ [\mathrm{ns}/\mathrm{tdc}\ ] + \mathrm{Offset}\ [\mathrm{ns}] - t_{\mathrm{reference}}. \tag{4.4}$$

The offset value includes several effects for each cell: The TDC pedestal values, the propagation time of the signal and the longitudinal time of flight of the muons from the trigger signal to the cell.

### Non-Linearity Correction

As the TDC-ramp may not be completely linear a phenomenological non-linearity correction is applied similar to [1] using a 2$^{nd}$-order polynomial fit. Figure 2(b) shows the residuals of the linear fit for a representative channel together with the fit that is used for the non-linearity correction.

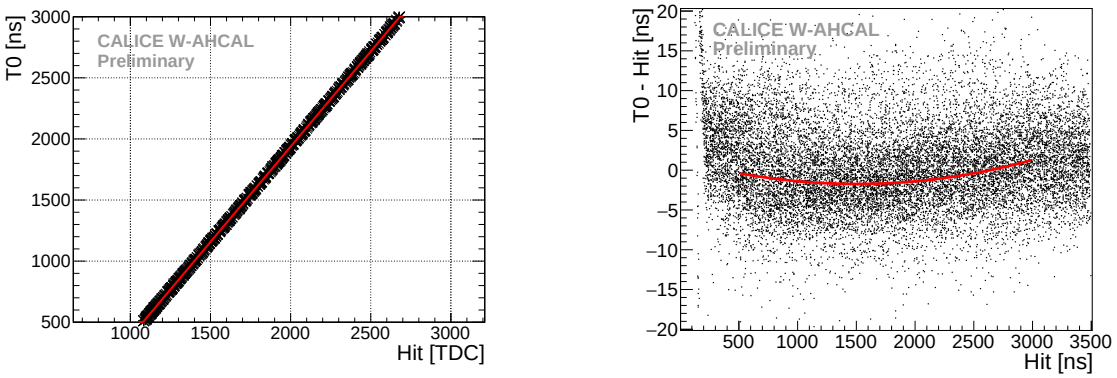


(a) (b)

Figure 2: (a) Linear fit between TDC-values of hits and reference time of the event shown for one representative channel. (b) 2$^{nd}$-order polynomial fit to the residuals of the linear fit for the non-linearity correction.

### Time Walk Correction

In order to correct for the fact that signals with a higher amplitude are expected to cross a constant threshold earlier than hits with a lower amplitude, a time walk correction is applied. The average hit time with respect to the hit energy is presented in fig. 3. The fit to the data is used as a correction of the hit time depending on the hit energy.

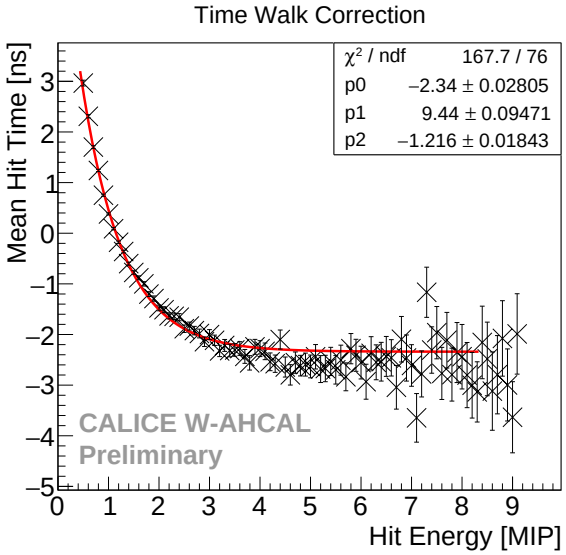


Figure 3: Average hit time dependent on the hit energy. The distribution is fitted with an exponential function of the form: $p_0 + p_1 * e^{p_2 * x}$. The small deviations of the data from the fits have no effect on the results.

## 5. Results

This section discusses the time distribution for muon, electron and pion data. The muon data is used to calibrate the detector and to extract the parameters for the time smearing of Monte Carlo (MC) hits. The calibration is cross-checked with electron data and further corrections are applied to account for the observed occupancy dependence of the time resolution as reported in [1]. Furthermore, the complex time structure of hadronic showers is discussed for pion data.

### 5.1 Muons

The time distribution of muon hits after calibration is shown in fig. 4. The time resolution is 6.3ns (RMS, in the interval $[-50\,\text{ns}, 50\,\text{ns}]$) , or 10.3 ns FWHM.

The muon hit time distribution is used as an input for the time smearing of the MC simulation [2]. For this purpose the hit time distribution is parametrized by a double gaussian fit:

$$t_{\text{muon}} = \frac{A_1}{A_1 + A_2} * \text{gaus}\,(\mu_1, \sigma_1) + \frac{A_2}{A_1 + A_2} * \text{gaus}\,(\mu_2, \sigma_2) \tag{5.1}$$

with the parameters specified in table 1. The double gaussian function is selected for parametrization in order to take the empirical larger tails of the distribution into account.

### 5.2 Electrons

Electromagnetic showers are, as well as muon hits, expected to give instantaneous signals with respect to the achievable time resolution. Thus, they can be used to cross-check the muon time calibration. The hit time distribution for data and MC for 20 GeV electrons is shown in fig. 5.

[2] Geant4 10.1, Mokka v08-05

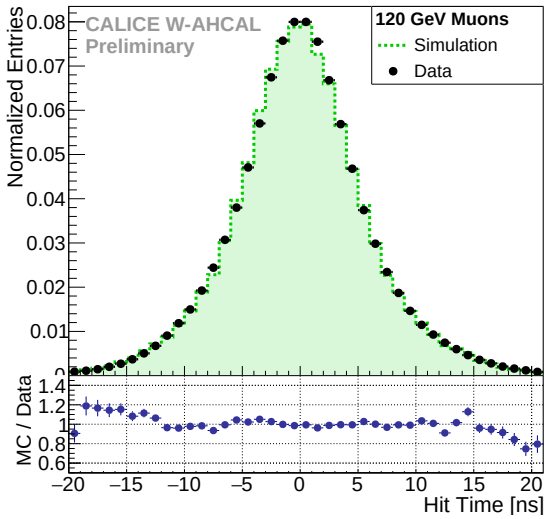


Figure 4: Muon hit time distribution. Comparison of data (black) and `QGSP_BERT_HP` (green).

Table 1: Parameters used as input for the time smearing of the MC simulation with eq. (5.1)

| | | |
|---|---|---|
| $A_1$ | $66.8 \times 10^3$ | $\pm\ 0.3 \times 10^3$ |
| $\mu_1$ | $-0.14$ ns | $\pm\ 0.01$ ns |
| $\sigma_1$ | 3.61 ns | $\pm\ 0.02$ ns |
| $A_2$ | $39.8 \times 10^3$ | $\pm\ 0.4 \times 10^3$ |
| $\mu_2$ | 0.24 ns | $\pm\ 0.01$ ns |
| $\sigma_2$ | 7.39 ns | $\pm\ 0.02$ ns |

It is significantly broadened compared to MIP-like particles, which is due to a problem with the readout ASICs that occurs for high channel occupancies in the ASIC. This effects manifests itself in two ways. First, a pedestal shift in the TDC-ramp is observed which leads to a time shift (see fig. 6(a)). Second, the hit time distribution is significantly broadened for events with a high ASIC occupancy. The shift can be easily corrected in data using the fit shown in fig. 6(a). The broadening of the hit time distribution cannot be corrected but has to be included in the digitization of the MC simulation hits. In order to take this effect into account the double gaussian fit explained in section 5.1 is convoluted by another gaussian distribution. The width of this additional gaussian depending on the ASIC occupancy is shown in Figure 6(b) and is used as an additional parameter for the time smearing of MC hits. For two layers (5 and 6) these effects are so severe that their hit time distributions cannot be recovered at all and thus they are excluded from further analysis. Both effects, the shift and the broadening, are consistent with the observations of the data with the steel absorber [1].

The electron hit time distribution after applying these corrections is shown in fig. 5. The time resolution for electrons is 10.2 ns RMS, or 19.1 ns FWHM.

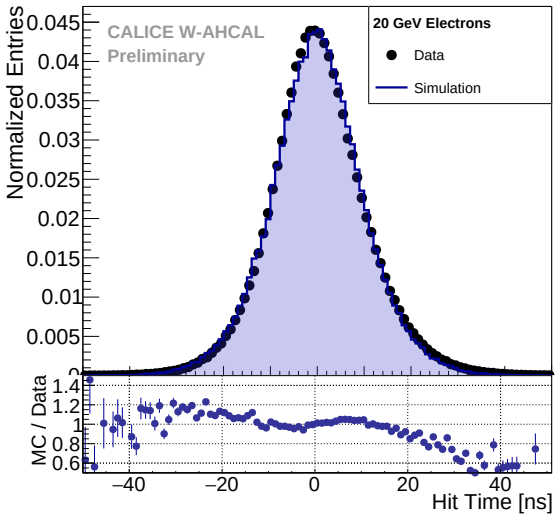


Figure 5: Distribution of hit times of 20 GeV electrons for data (black) and QGSP_BERT_HP (purple), with corrections due to high ASIC occupancies.

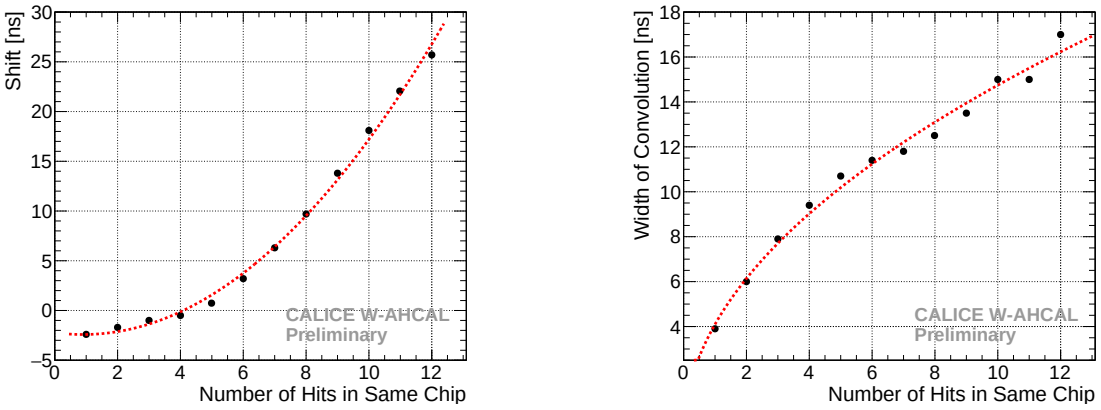


(a) (b)

Figure 6: Correction to the hit time depending on the ASIC occupancy. The observed shift in the hit time distribution (a) is corrected for and the broadening of the hit time distribution (b) is implemented in the time smearing of the MC hit times. A quadratic and a square root function are added to the plots respectively to guide the eye.

### 5.3 Pions

The time distribution of hadronic showers is shown in fig. 7(a). Compared to electromagnetic showers discussed in the previous section, a late tail in the distribution is visible. The production of slow neutrons in the hadronic part of the shower leads to two processes that produce delayed hits. On timescales of the order of a few ns, neutron-proton elastic scattering is the dominant process, while energy depositions due to neutron capture can extend to several µs after the primary particle hits the calorimeter. Taking systematic and geometric effects into account the results are compatible

with the results presented by the T3B experiment in [6]. The distribution is consistent over the whole energy range, meaning that the fraction of late hits does not depend on the energy of the incoming particles, as expected. The slight broadening of the distribution between 50 ns and 120 ns is due to the effects described in section 5.2. As higher energetic particles produce more hits, the average occupancy of the ASICs is higher in this case resulting in a wider distribution.

A comparison of data with MC simulations is exemplified by 70 GeV pions for different physics lists in fig. 7(b). It shows a sorting of the physics lists into two categories depending on the model that is used for low energetic particles. Physics lists as `QGSP_BERT_HP` that rely on the Bertini model [7] show significantly more hits with hit times $> 100$ ns. `QBBC` and `QGSP_BIC` use a binary cascade model for the propagation of low energetic particles. For them less of these late hits are observed compared to data. `QGSP_BIC_HP` that uses the high precision neutron model shows a similar behavior as the `QGSP_BERT`-like models.

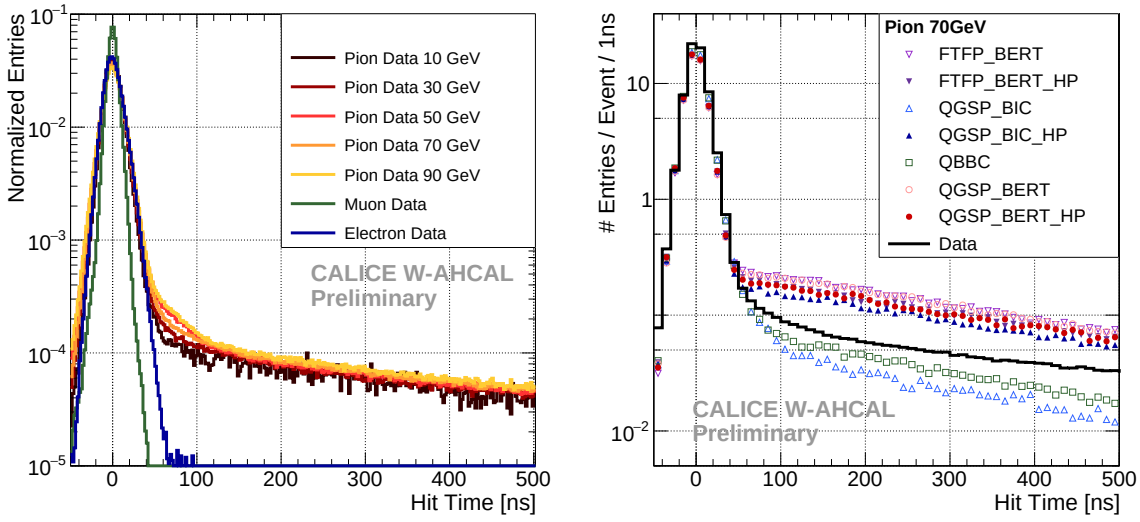


(a) (b)

Figure 7: (a) Distribution of hit times for 10 GeV to 90 GeV pions, 120 GeV muons and 20 GeV electrons. Distributions are normalized to 1. (b) Distribution of hit times of 70 GeV pions for data (black) compared to several Geant4 physics lists and normalized to the number of hits per 10 ns per event.

The distribution of the fraction of hits in an event that are later than 75 ns is shown in fig. 8(a). Data is compared with three physics lists: `QGSP_BERT` as a representative using the Bertini model, `QGSP_BERT_HP` using the HP package for low energetic neutrons and `QBBC` relying on the binary-cascade model. In data the most probable value is 5 % hits later than 75 ns. For `QBBC` the distribution is slightly shifted to lower values with significantly more events that do not have a late hit at all, while the distribution for `QGSP_BERT(_HP)` is shifted to higher values with the most probable value being around 13 % (15 %).

Figures 8(b), 8(c) and 8(d) show the distribution of the average fraction of late hits over the position in $z$-direction, the hit radius (radial distance to center of gravity of the event) and the hit energy. It can be seen that the late hits are consistently distributed over all layers. The `QBBC`

physics list is missing some of the late hits especially in the last layer. Low energy depositions have a large fraction of late hits (up to 8 % for hit energies between 0.5 MIP and 1.0 MIP). Large energy depositions above 5 MIP are again dominated by the electromagnetic part of the shower and thus show nearly no content of late energy depositions. While the center of the shower is dominated by the quasi-instantaneous electromagnetic shower, the outer part of the shower consists to a large extent of late energy depositions (up to 25 % for data at hit radii close to 300 mm). The `QGSP_BERT(_HP)` physics lists have consistently more late hits distributed over all hit radii and hit energies compared to data, while `QBBC` is missing late hits mostly for low energy depositions ($< 3$ MIP) at large hit radii ($> 120$ mm).
Appendix 10 in appendix B shows the lateral shower shape as well as the hit radius distributions for early and late hits. It can be seen that the instantaneous part is well described by all physics lists. Also the shape of the hit radius distribution for late hits agrees between data and the `QGSP_BERT(_HP)` physics lists. The `QBBC` physics list however has more late hits in the center of the shower and less in the outer part.

**Discussion of Uncertainties**

Statistical errors are in general low for the distributions shown in this section and thus not drawn in order to maintain readability of the plots. For systematic errors, various effects have to be discussed:

- Calibration: For the calibration a high precision is observed. Uncertainties in the calibration and time walk corrections are expected to be much smaller than 1 ns on average. However, especially at the outer part of the detector, not all channels can be calibrated properly, which may lead to uncertainties of a few nanoseconds for those channels.
- Occupancy correction: The occupancy correction may lead to uncertainties of a few nanoseconds, especially for high chip occupancies where less data is available to estimate the correction parameters.
- Multi-particle events: Multi-particle events are efficiently rejected in the event selection.
- Noise: The noise hit rates are well below the rate of late neutrons. This is checked with muon runs.

The total systematic uncertainties are of the order of a few nanoseconds, dominated by the chip occupancy correction, and too small to be visible in fig. 7. For fig. 8, the fraction of hits later than a fixed threshold is used as a metric to compare data and MC. The threshold of 75 ns is chosen in such a way, that systematic uncertainties have a minimal impact on the results. In order to check the robustness of this measure, the mean number of late hits is compared for thresholds of 70 ns, 75 ns and 80 ns. The mean fraction of late hits varies relatively by less than 1 % for these values.

**Comparison to Steel Absorber**

As tungsten has a higher atomic number than steel, more hadronic interactions are expected with a tungsten absorber compared to a steel absorber leading to more produced low energetic neutrons and thus to more late hits. The time analysis of the technological prototype with a steel absorber is described in [1]. Figure 9 shows the time distribution of 50 GeV pions with a tungsten and steel absorber. In tungsten the late tail of the distribution is enhanced by about a factor eight on average.

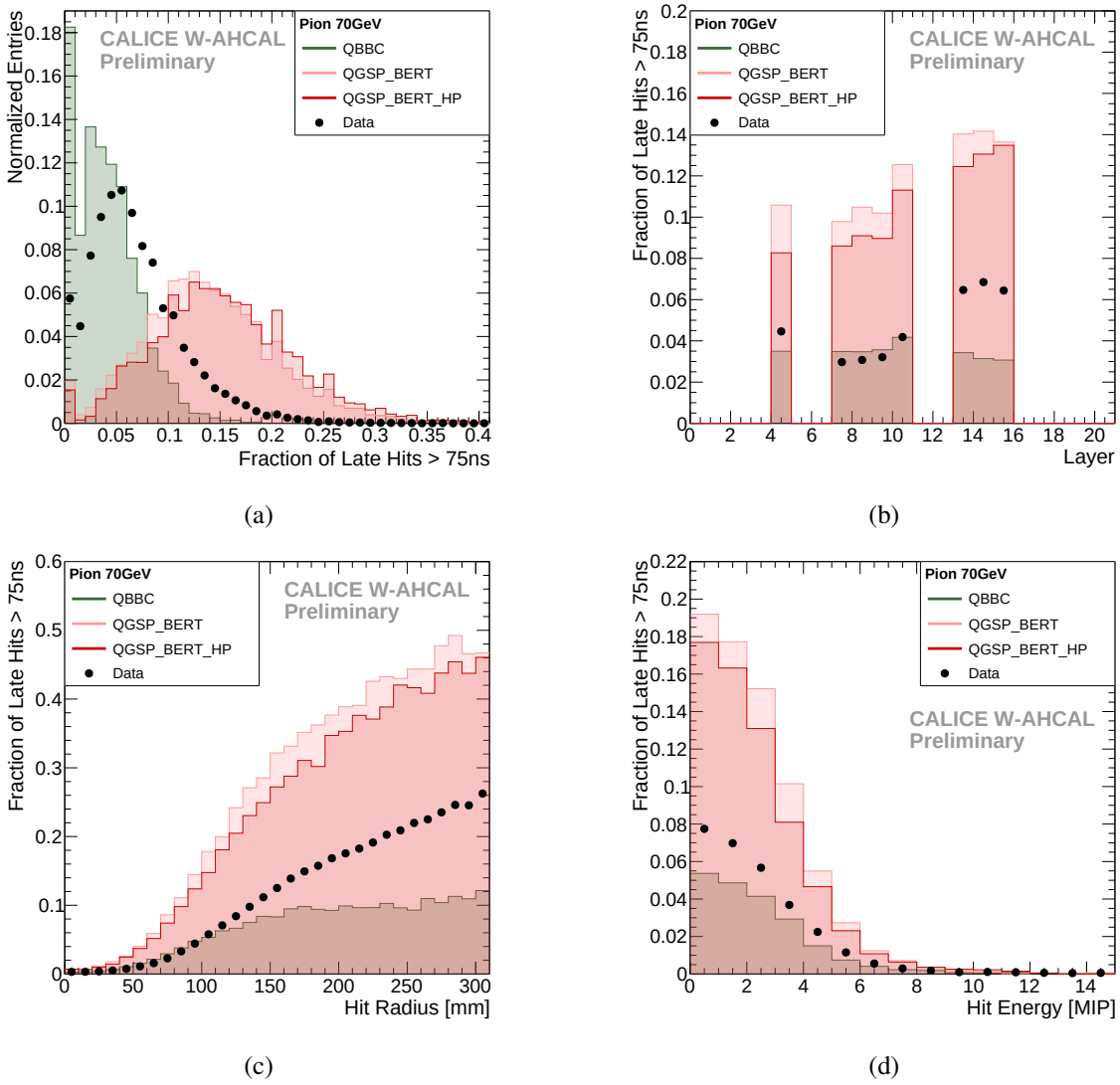


Figure 8: (a) Distribution of the fraction of hits in each event that are later than 75 ns, the fraction of late hits distributed over layers (b), hit radii (c) and hit energies (d). Comparison of data (black) with QGSP_BERT (light red), QGSP_BERT_HP (dark red) and QBBC physics list (green).

### Comparison to the T3B Experiment

In T3B, good agreement is observed for QBBC and QGSP_BERT_HP with a tungsten absorber, while a large discrepancy for late hits is seen for QGSP_BERT, based on simulations with Geant4 9.4 [8]. In the presently used Geant4 version 10.1 substantial changes have been implemented in nearly all physics lists. The neutron capture cross-sections and the neutron final state model of QBBC have been adopted by QGSP_BIC, QGSP_BERT and FTFP_BERT. Also QBBC itself underwent changes especially in the low and medium energy regions (< 12 GeV) for hadronic interactions [9]. In addition, the T3B experiment had a special geometry. It was located at the very end of the physics prototype probing on average a different depth of the shower, as well as giving more weight to hits near the center of the shower, due to the strip geometry of the experiment. As a cross-check, a toy

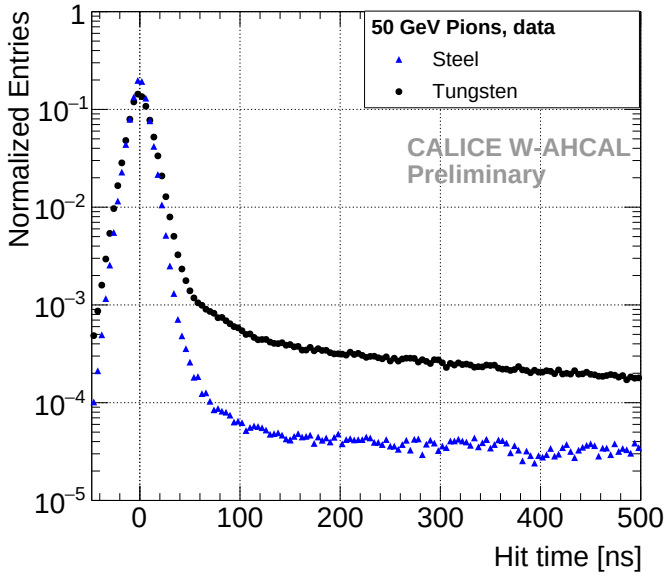


Figure 9: Comparison of the time distribution of 50 GeV pions between data with a tungsten absorber (blue) and a steel absorber (black).

Monte Carlo experiment was set up to check the influence of the different Geant4 versions as well as geometric effects. Even though it is difficult to directly compare the two experiments due to many systematic differences, the observed results of the toy MC are consistent with the differences between the T3B results and the analysis presented in this note.

## 6. Conclusion

This note analyzes data of the AHCAL test beam campaign in August 2015 at the SPS at CERN. The focus of this analysis lies on the time measurements of hadronic showers with tungsten as the absorber material. For this a time calibration procedure is established. For muons a time resolution of about 6 ns is achieved. The muon time resolution is used as a time smearing for MC simulation. For electrons a worse time resolution of 10 ns is observed, due to a malfunctioning of the front-end electronics at high hit occupancies.

For pions late, low energy hits are visible as it is expected due to low energetic neutrons. In comparison with MC simulation of several physics lists, it turns out that models that rely on the binary cascade for hadronic processes of low energetic particles are underestimating these late energy depositions, while models that use the Bertini model and the high precision neutron package are overestimating this part by about a factor two. Comparing the results of this analysis with a similar analysis using data with a steel absorber, significantly more late energy depositions are observed in tungsten, which is expected because of the higher atomic number of tungsten.

## References


[1] E. Brianne, *Time Development of Hadronic Showers in a Highly Granular Analog Hadron Calorimeter*. PhD thesis, DESY, Hamburg, Germany, 2018.

[2] F. Simon, C. Soldner, and L. Weuste, *T3B - An Experiment to Measure the Time Structure of Hadronic Showers*, *JINST* **8** (2013), no. 12 P12001.

[3] D. Dannheim, W. Klempt, and E. van der Kraaij, *Beam Tests with the CALICE Tungsten Analog Hadronic Calorimeter Prototype*, *LCD-Note-2012-002* (Apr, 2012).

[4] [CALICE], C. Adloff, *et. al.*, *Shower Development of Particles with Momenta from 1 to 10 GeV in the CALICE Scintillator-Tungsten HCAL*, *JINST* **9** (2014), no. 01 P01004.

[5] D. Lorenzo *et. al.*, *SPIROC: Design and Performances of a Dedicated very Front-end Electronics for an ILC Analog Hadronic CALorimeter (AHCAL) Prototype with SiPM Read-out*, *JINST* **8** (2013), no. 01 C01027.

[6] [CALICE], C. Adloff, *et. al.*, *The Time Structure of Hadronic Showers in Highly Granular Calorimeters with Tungsten and Steel Absorbers*, *JINST* **9** (2014), no. 07 P07022.

[7] J. Apostolakis *et. al.*, *GEANT4 Physics Lists for HEP*, *2008 IEEE Nuclear Science Symposium Conference Record* (2008).

[8] F. Simon *et. al.*, *The Time Structure of Hadronic Showers in Imaging Calorimeters with Scintillator and RPC Readout*, *arXiv preprint arXiv:1308.6395* (2013).

[9] A. Ribon, *private communication*, .

# Appendices

## A. Layer Configuration

Table 2: Physical ordering of layers in the AHCAL tungsten technological prototype for the August 2015 testbeam campaign. Additionally, the SiPM and tile configuration is given.

| Phys. Order | Abs. Layer | Type | SiPM | Scintillator |
|---|---|---|---|---|
| 1 | 0 | 1 × EBU | Hamamatsu 10 000 px | strips |
| 2 | 1 | 1 × EBU | Hamamatsu 10 000 px | strips |
| 3 | 2 | 1 × EBU | Hamamatsu 1600 px | strips |
| 4 | 3 | 1 × HBU | Hamamatsu 1600 px | tiles w/ surf. mount SiPMs |
| 5 | 4 | 1 × HBU | Ketek 12 000 px | tiles w/o WLS fibres |
| 6 | 5 | 1 × HBU | Ketek 12 000 px | tiles w/o WLS fibres |
| 7 | 6 | 1 × HBU | CPTA 800 px | tiles w/ WLS fibres |
| 8 | 7 | 1 × HBU | CPTA 800 px | tiles w/ WLS fibres |
| 9 | 8 | 1 × HBU | CPTA 800 px | tiles w/ WLS fibres |
| 10 | 9 | 1 × HBU | CPTA 800 px | tiles w/ WLS fibres |
| 11 | 10 | 1 × HBU | CPTA 800 px | tiles w/ WLS fibres |
| 12 | 11 | 4 × HBU | Ketek 2300 px | tiles w/o WLS fibres |
| 13 | 13 | 4 × HBU | Ketek 2300 px | tiles w/o WLS fibres |
| 14 | 21 | 4 × HBU | SenSL 1300 px | tiles w/o WLS fibres |
| 15 | 31 | 4 × HBU | SenSL 1300 px | tiles w/o WLS fibres |

## B. Additional Plots: Lateral Shower Shape

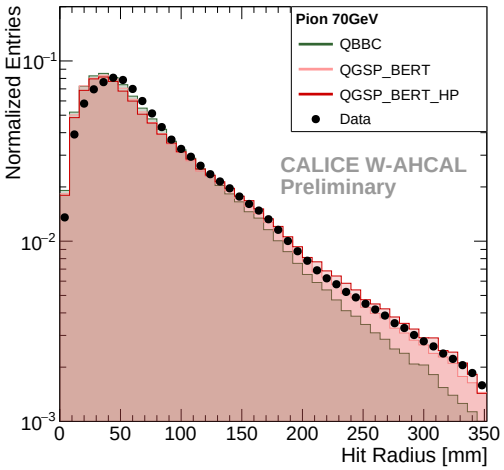


(a) Hit radius distribution

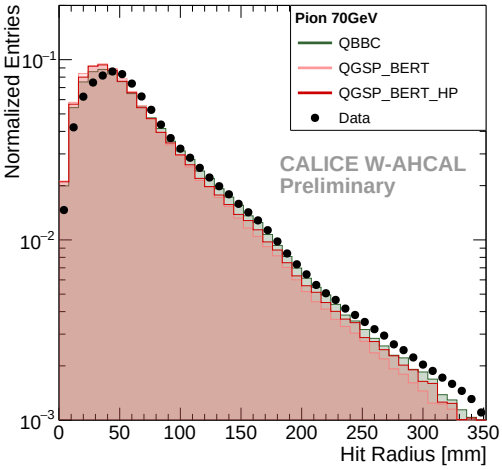


(b) Hit radius distribution for early hits <= 75 ns

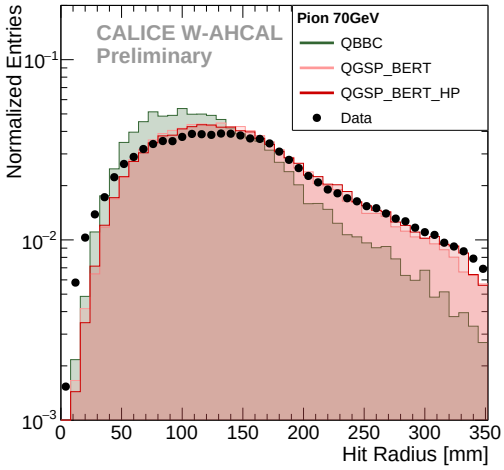


(c) Hit radius distribution for late hits > 75 ns

Figure 10: Hit radius distribution of data compared to MC simulation using different physics lists (a). The data is split up in early hits <= 75 ns (b) and late hit > 75 ns (c).